Penetration Through Slots in Conducting Cylinders—Part 1: TE Case

John D. Shumpert, *Student Member, IEEE*, and Chalmers M. Butler, *Fellow, IEEE*

***Abstract*— Three methods for determining the penetration through small apertures in closed conducting surfaces are outlined and their salient features discussed. These methods are designated: 1) the scatterer method; 2) the short-circuit current method; and 3) the equivalent current method. They are implemented by integral equation techniques but are amenable to differential equation or hybrid methods. Procedures for applying each method are outlined, as are schemes for repairing singular equations rendered invalid by the presence of false resonances. Reasons for inaccuracies in the three methods are also delineated. Data determined for a given structure by all three methods are presented and numerical examples that illustrate important features of the methods and their relative accuracies are described. It is pointed out that some methods yield incorrect penetration data. In this part of the paper, is found an outline of the integral equation formulations and numerical schemes needed to accurately determine the field that penetrates through a slot in a conducting cylinder excited by an axially independent TE source. In Part 2, the TM case is presented.**

***Index Terms*—Apertures, electromagnetic coupling, numerical analysis.**

I. Introduction

ONE of the problems that researchers have been interested in for several years is that of computing fields that penetrate via very small apertures through conducting surfaces. (An extensive bibliography appears in [1].) In particular, we are concerned with the determination of the field that penetrates through slots in conducting cylinders. The straightforward solution of this problem in which one simply treats the body as a scatterer and determines the interior field as the sum of the incident field and the scattered field contributed by the current induced on the body surface, can yield inaccurate results if the aperture is very small or is a thin slit oriented on the body surface in such a way that the leakage is small. Alternate integral equations methods, namely what we have termed the *short-circuit current method* and the *equivalent current method*, do yield accurate penetrated fields, but they fail at the internal resonances of the *equivalent* closed body, even though the interior region of the body is not actually a cavity with a complete impenetrable boundary. Because the alternate methods are susceptible to interior resonance difficulties, which are not easy to avoid directly when bodies are of complex shape, we propose still additional formulations that remain valid over the entire spectrum of interest.

Unfortunately, the two alternate methods themselves suffer from inherent difficulties and often entail far more work and/or require greater computer resources than does the scatterer method; and they are not equally easy to apply to complex structures. Through the judicious choice of equivalent sources and appropriate basis functions, some of these difficulties can be remedied. For example, one can devise a variation of an aperture method involving only equivalent electric currents (but with no magnetic current as is typical in the traditional implementation of this solution procedure) to enable one to determine the total field both inside and outside a conducting body with a hole in its surface.

Although the classic problem of determining the electromagnetic scattering by conducting cylinders with axial slots has been investigated by many researchers [2], [3] using a variety of techniques, the determination of the penetrated field through slots in conducting cylinders has received little attention. Senior [4], [5] investigated the field inside infinite, conducting slotted circular cylinders due to an E-polarized (TM to cylinder axis) incident plane wave. Schuman and Warren [6] applied the Schelkunoff equivalence principle [7] to bodies of revolution in order to improve the accuracy of field computations for cases when the aperture is small and/or when the field at points deep within the cavity is sought. A hybrid technique combining the frequency-domain method of moments and the finite-difference time-domain (FDTD) method has been employed by Taflove and Umashankar [8] to solve various penetration problems. Beren [9] implemented the aperture field integral equation (AFIE), electric field integral equation (EFIE), and H-field integral equation (HFIE) to determine fields in and around an axially slotted cylinder. Johnson and Ziolkowski [10] developed a generalized dual-series solution of an H-polarized plane wave incident on a circular cylinder with an axial slot. Ziolkowski *et al.* [11], [12] produced extensive contour plots for the field penetration of E- and H-polarized plane waves incident on concentrically loaded, slotted cylinders using the dual series approach developed in [10]. Recently, Mautz and Harrington calculated the electromagnetic field in the vicinity of a vanishingly thin conducting circular cylindrical shell with an axial slot due to

Manuscript received December 4, 1995; revised September 8, 1997. This work was supported by the U.S. Army Research Office under Grant DAAL03-92-G-0376 and by the National Science Foundation through its Graduate Fellowship Program.

J. D. Shumpert was with the Department of Electrical and Computer Engineering, Clemson University, Clemson, SC 29634 USA. He is now with the Radiation Laboratory, Department of Electrical Engineering and Computer Science, University of Michigan, Ann Arbor, MI 48109 USA.

C. M. Butler is with the Department of Electrical and Computer Engineering, Clemson University, Clemson, SC 29634 USA.

Publisher Item Identifier S 0018-926X(98)08879-6.

both TE [13] and TM [14] polarizations. Butler [15] investigated the field penetration into conducting circular cylinders with small apertures for both polarizations. Our research is primarily focused on methods for determining the field which penetrates conducting cylinders with arbitrary contours containing infinitely long narrow axially directed slots.

In Section II, the solution methods are described and integral equations are derived that, when solved, yield currents from which penetrated field can be determined. These equations are developed for the: 1) scatterer method; 2) short-circuit current method; and 3) equivalent current method. Procedures for applying each method are outlined as are schemes for repairing singular equations rendered invalid by the presence of false resonances. In Section III, moment-method solutions are developed to solve the integral equations derived in Section II. It is pointed out that some methods yield incorrect interior fields when the level of penetration is small and what must be done to obtain correct fields is discussed. Data determined for a given structure by all three methods are presented and numerical examples that illustrate important observations about the methods and their relative accuracies are described in Section IV. The TM case formulation, numerical scheme, and pertinent data are presented in Part 2.

II. Formulation of Integral Equations

Three methods for determining penetrated field through slots in conducting cylinders are outlined and procedures for applying the methods are delineated. The first, the scatterer method, treats the body as a scatterer and determines the interior field as the sum of the incident field produced by a known source and the scattered field contributed by the current induced on the body. The second, the short-circuit current method, is based upon a field equivalence theorem due to Schelkunoff [7], which allows one to change the excitation of the structure from the known source or incident field to an equivalent surface current placed in the aperture. The penetrated field can then be determined by a procedure similar to that of the scatterer method but without the inherent inaccuracies. The third, the equivalent current method, employs the equivalence principle [16] to solve for equivalent magnetic currents and then determines the penetrated field from knowledge of these currents.

A. Scatterer Method

The scatterer method is the simplest technique for computing the field that penetrates through an aperture in a conducting surface. A representative body with conducting surface $\mathcal{S}$ and aperture $\mathcal{A}$ is illustrated in cross section in Fig. 1. In this method, the body is treated as a scatterer and the penetrated field is determined as the sum of the incident field produced by a known source and the scattered field contributed by the current induced on the body. The total electric field can be viewed as the sum of an incident field $\mathbf{E}^i(\mathbf{r})$ due to radiation from a known source with the scatterer absent and a scattered field $\mathcal{E}[\mathbf{J};\mathbf{r};\Sigma]$, which is due to radiation by the current on a surface Σ

$$\mathbf{E}(\mathbf{r}) = \mathcal{E}[\mathbf{J};\mathbf{r};\Sigma] + \mathbf{E}^i(\mathbf{r}) \tag{1}$$

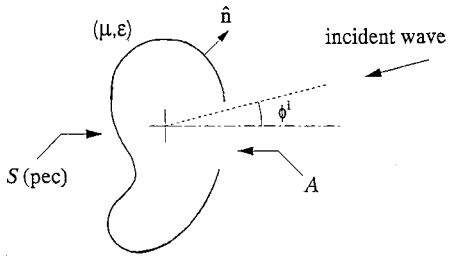

Fig. 1. General conducting surface with opening excited by known source.

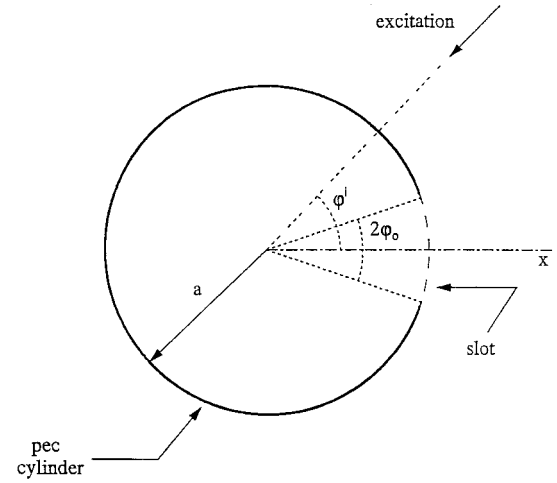

Fig. 2. Cross-sectional view of axially slotted circular conducting cylinder of radius a and slot angle $2\phi_o$ excited by plane wave.

in which the operator $\mathcal{E}[\mathbf{J};\mathbf{r};\Sigma]$ can be expressed in terms of potentials as

$$\mathcal{E}[\mathbf{J};\mathbf{r};\Sigma] = -j\omega\mathbf{A}(\mathbf{r}) - \nabla\Phi(\mathbf{r}) \tag{2}$$

with

$$\begin{aligned}\mathbf{A}(\mathbf{r}) &= \mu\iint_{\Sigma}\mathbf{J}(\mathbf{r}')G(\mathbf{r};\mathbf{r}')\,dS',\\ \Phi(\mathbf{r}) &= \frac{j\eta}{k}\iint_{\Sigma}(\nabla_s'\cdot\mathbf{J}(\mathbf{r}'))G(\mathbf{r};\mathbf{r}')\,dS'\end{aligned} \tag{3}$$

where $G(\mathbf{r};\mathbf{r}')$ is the free-space Green's function $\eta = \sqrt{\mu/\varepsilon}$, $k = \omega\sqrt{\mu\varepsilon}$ and Σ represents a generic or dummy surface on which sources reside. The field must satisfy

$$\mathcal{E}_{\tan}[\mathbf{J};\mathbf{r};\Sigma] + \mathbf{E}^i_{\tan}(\mathbf{r}) = \mathbf{0}, \quad \mathbf{r}\in\mathcal{S} \tag{4}$$

on the conducting surface where the subscript "tan" denotes the tangential component of the operator or field on the surface $\mathcal{S}$.

Consider the slotted cylinder shown in Fig. 2 excited by an incident plane wave propagating in a direction normal to the z axis with its magnetic field parallel to the axis (TE$_z$). For such an excitation, the induced electric current $\mathbf{J}$ has only a component in the $\hat{\mathbf{l}}$ direction where $\hat{\mathbf{l}}$ is a unit vector tangential to the contour in the transverse plane that is defined at a surface point by $\hat{\mathbf{l}} = \hat{\mathbf{z}}\times\hat{\mathbf{n}}$ in terms of the axial direction $\hat{\mathbf{z}}$ and the unit normal $\hat{\mathbf{n}}$ outward from the surface. In light of (4), an EFIE

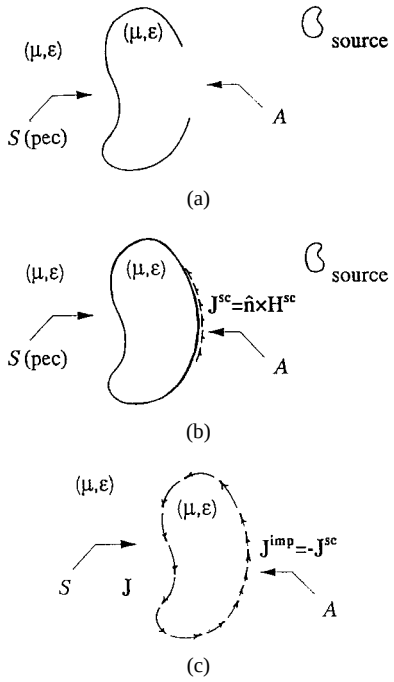

Fig. 3. Illustrations for the short-circuit current method. (a) Original structure. (b) Short-circuit current over aperture region. (c) Equivalent model.

can be formulated to determine the induced electric current on the scatterer

$$\frac{\eta}{4k}\left[k^2\int_{C_S} J_l(\boldsymbol{\rho}')\hat{\mathbf{l}}\cdot\hat{\mathbf{l}}' H_0^{(2)}(k|\boldsymbol{\rho}-\boldsymbol{\rho}'|)\,dl' + \frac{d}{dl}\int_{C_S}\frac{d}{dl'}J_l(\boldsymbol{\rho}')H_0^{(2)}(k|\boldsymbol{\rho}-\boldsymbol{\rho}'|)\,dl'\right] = \hat{\mathbf{l}}\cdot\mathbf{E}^i(\boldsymbol{\rho}), \quad \boldsymbol{\rho}\in C_S \tag{5}$$

where C_S is the contour of the conductor and where $\frac{d}{dl}$ is the directional derivative along C_S in the $\hat{\mathbf{l}}$ direction. The subscript "l" is appended to quantities to indicate the vector component in the $\hat{\mathbf{l}}$ direction. The two-dimensional Green's function in cylindrical coordinates is $\frac{1}{4j}H_0^{(2)}(k|\boldsymbol{\rho}-\boldsymbol{\rho}'|)$ where $H_0^{(2)}(\cdot)$ is the zeroth-order cylindrical Hankel function of the second kind. The total electric field is computed as the sum of the scattered field produced by the induced electric current found in (5) and the incident electric field. Given $\mathbf{H}^i = \hat{\mathbf{z}}H_o^i e^{jk(x\cos\phi^i+y\sin\phi^i)}$, the corresponding incident electric field $\mathbf{E}^i$ is

$$\mathbf{E}^i = (\hat{\mathbf{z}}\times\hat{\mathbf{k}})E_o^i e^{jk(x\cos\phi^i+y\sin\phi^i)} \tag{6}$$

which impinges upon the cylinder of Fig. 2 along a ray in the $\hat{\mathbf{k}} = -(\cos\phi^i\hat{\mathbf{x}}+\sin\phi^i\hat{\mathbf{y}})$ direction defined with the angle ϕ^i with respect to the x axis.

B. Short-Circuit Current Method

Schelkunoff developed field analogues of the Helmholtz–Thévenin and Norton circuit theorems that allow one to replace the effect of an aperture in the surface of a body shown in Fig. 3(a) with equivalent "impressed" currents in the aperture. In the short-circuit current method, we short the aperture and compute the short-circuit current induced on the equivalent *closed* surface $\mathcal{S}+\mathcal{A}$ depicted in Fig. 3(b). The short-circuit current $\mathbf{J}^{\rm sc}$ is determined from

$$-\mathcal{E}_{\tan}[\mathbf{J}^{\rm sc};\mathbf{r};\mathcal{S}+\mathcal{A}] = \mathbf{E}^i_{\tan}(\mathbf{r}), \quad \mathbf{r}\in\mathcal{S}+\mathcal{A} \tag{7}$$

where $\mathcal{E}[\mathbf{J};\mathbf{r};\Sigma]$ is given in (2). To overcome problems caused by false interior resonances, one may replace (7) by the corresponding combined field equation

$$-\hat{\mathbf{n}}\times\mathcal{H}^-[\mathbf{J}^{\rm sc};\mathbf{r};\mathcal{S}^-+A^-] - \frac{\alpha}{\eta}\mathcal{E}_{\tan}[\mathbf{J}^{\rm sc};\mathbf{r};\mathcal{S}+\mathcal{A}] = \hat{\mathbf{n}}\times\mathbf{H}^i(\mathbf{r}) + \frac{\alpha}{\eta}\mathbf{E}^i_{\tan}(\mathbf{r}), \quad \mathbf{r}\in\mathcal{S}^-+\mathcal{A}^- \tag{8}$$

where $\mathcal{E}[\mathbf{J};\mathbf{r};\Sigma]$ is given in (2) and, $\mathcal{H}[\mathbf{J};\mathbf{r};\Sigma]$ is given by

$$\mathcal{H}[\mathbf{J};\mathbf{r};\Sigma] = \frac{1}{\mu}\nabla\times\mathbf{A}(\mathbf{r}) = \iint_{\Sigma^-}\mathbf{J}(\mathbf{r}')\times\nabla'_s G(\mathbf{r};\mathbf{r}')\,dS', \quad \mathbf{r}\neq\mathbf{r}'. \tag{9}$$

$\hat{\mathbf{n}}$ is the outward normal to $\mathcal{S}$ at $\mathbf{r}$ and α is a multiplicative parameter that is usually chosen to be in the range $0.2\le\alpha\le 1$ [17]. The minus superscript in (8) indicates that the magnetic field must be evaluated in the limit as the field point $\mathbf{r}$ approaches the surface electric current along a path in the interior region.

Knowing $\mathbf{J}^{\rm sc}$ from the solution of (7) or (8), we return to the original structure of Fig. 3(a), with the short and external source removed and, following Schelkunoff, impress in the aperture a known current $\mathbf{J}^{\rm imp} = -\mathbf{J}^{\rm sc}$ in which $\mathbf{J}^{\rm sc}$ is the short-circuit current over $\mathcal{A}$. The equivalent E-field excitation in the interior region can be found from

$$\mathbf{E}^{\rm imp}(\mathbf{r}) = \mathcal{E}[+\mathbf{J}^{\rm imp};\mathbf{r};\mathcal{A}] = \mathcal{E}[-\mathbf{J}^{\rm sc};\mathbf{r};\mathcal{A}]. \tag{10}$$

The new problem is then solved by treating the conducting body as a scatterer with surface $\mathcal{S}$ excited by the current source $\mathbf{J}^{\rm imp}$ as suggested in Fig. 3(c). The resulting induced current $\mathbf{J}$ on the conductor (different from the current found in Section II-A) can be determined by solving

$$-\mathcal{E}_{\tan}[\mathbf{J};\mathbf{r};\mathcal{S}] = \mathbf{E}^{\rm imp}_{\tan}(\mathbf{r}), \quad \mathbf{r}\in\mathcal{S}. \tag{11}$$

The interior (penetrated) field is the sum of the field produced directly by the current source $\mathbf{J}^{\rm imp}$ and the scattered field contributed by the current $\mathbf{J}$ induced on the conducting surface

$$\mathbf{E}^{\rm pen}(\mathbf{r}) = \mathcal{E}[\mathbf{J};\mathbf{r};\mathcal{S}] + \mathcal{E}[\mathbf{J}^{\rm imp};\mathbf{r};\mathcal{A}]. \tag{12}$$

To compute the short-circuit current over the aperture region, an equation similar to (5) can be enforced over the entire cylinder with the slot shorted

$$\frac{\eta}{4k}\left[k^2\int_{C_S+C_A} J_l^{\rm sc}(\boldsymbol{\rho}')\hat{\mathbf{l}}\cdot\hat{\mathbf{l}}' H_0^{(2)}(k|\boldsymbol{\rho}-\boldsymbol{\rho}'|)\,dl' + \frac{d}{dl}\int_{C_S+C_A}\frac{d}{dl'}J_l^{\rm sc}(\boldsymbol{\rho}')H_0^{(2)}(k|\boldsymbol{\rho}-\boldsymbol{\rho}'|)\,dl'\right] = E_l^i(\boldsymbol{\rho}), \quad \boldsymbol{\rho}\in C_S+C_A \tag{13}$$

where E_l^i $(=\hat{\mathbf{l}}\cdot\mathbf{E}^i)$ is the l component of $\mathbf{E}^i$, C_S is the contour of the conductor, and C_A is the contour of the aperture. As

before, false resonances can be overcome by replacing (13) with the corresponding combined field integral equation

$$\frac{1}{2}J_l^{\rm sc}(\boldsymbol{\rho}) - \frac{k}{4j}\int_{C_S+C_A} J_l^{\rm sc}(\boldsymbol{\rho}')\cos\theta' H_1^{(2)}(k|\boldsymbol{\rho}-\boldsymbol{\rho}'|)\,dl' + \frac{\alpha}{4k}\left[k^2\int_{C_S+C_A} J_l^{\rm sc}(\boldsymbol{\rho}')\hat{\mathbf{l}}\cdot\hat{\mathbf{l}}' H_0^{(2)}(k|\boldsymbol{\rho}-\boldsymbol{\rho}'|)\,dl' + \frac{d}{dl}\int_{C_S+C_A}\frac{d}{dl'}J_l^{\rm sc}(\boldsymbol{\rho}')H_0^{(2)}(k|\boldsymbol{\rho}-\boldsymbol{\rho}'|)\,dl'\right] = -H_z^i(\boldsymbol{\rho}) + \frac{\alpha}{\eta}E_l^i(\boldsymbol{\rho}), \quad \boldsymbol{\rho}\in C_S+C_A \tag{14}$$

in which $H_z^i(\boldsymbol{\rho})$ is defined

$$H_z^i(\boldsymbol{\rho}) = H_o^i e^{jk(x\cos\phi^i + y\sin\phi^i)} \tag{15}$$

with $H_o^i = E_o^i/\eta$ for consistency with $\mathbf{E}^i$ of (6). $\hat{\mathbf{n}}'$ is the outward normal illustrated in Fig. 1 located at the source point defined by the vector $\boldsymbol{\rho}'$ and $\cos\theta' = \hat{\mathbf{u}}\cdot\hat{\mathbf{n}}'$ in which $\hat{\mathbf{u}} = (\boldsymbol{\rho}-\boldsymbol{\rho}')/|\boldsymbol{\rho}-\boldsymbol{\rho}'|$. In the event that the radius of curvature of a surface is discontinuous at $\boldsymbol{\rho}$, $\frac{1}{2}J_l^{\rm sc}$ must be replaced by $\frac{\beta}{2\pi}J_l^{\rm sc}$ where β is the angle of the indentation or protrusion of the surface at $\boldsymbol{\rho}$ as defined in [18].

Using the aperture short-circuit current found in (13) or (14), we solve the new problem by treating the body as a scatterer and determining the induced current $\mathbf{J} = J_l\hat{\mathbf{l}}$ on the scatterer from

$$\frac{\eta}{4k}\left[k^2\int_{C_S} J_l(\boldsymbol{\rho}')\hat{\mathbf{l}}\cdot\hat{\mathbf{l}}' H_0^{(2)}(k|\boldsymbol{\rho}-\boldsymbol{\rho}'|)\,dl' + \frac{d}{dl}\int_{C_S}\frac{d}{dl'}J_l(\boldsymbol{\rho}')H_0^{(2)}(k|\boldsymbol{\rho}-\boldsymbol{\rho}'|)\,dl'\right] = -\frac{\eta}{4k}\left[k^2\int_{C_A} J_l^{\rm imp}(\boldsymbol{\rho}')\hat{\mathbf{l}}\cdot\hat{\mathbf{l}}' H_0^{(2)}(k|\boldsymbol{\rho}-\boldsymbol{\rho}'|)\,dl' + \frac{d}{dl}\int_{C_A}\frac{d}{dl'}J_l^{\rm imp}(\boldsymbol{\rho}')H_0^{(2)}(k|\boldsymbol{\rho}-\boldsymbol{\rho}'|)\,dl'\right], \quad \boldsymbol{\rho}\in C_S \tag{16}$$

where the right-hand side of (16) is the negative of the l component of the known E field excitation due to $\mathbf{J}^{\rm imp}$ $(=-\mathbf{J}^{\rm sc})$.

It is important to understand the behavior of the current at a slot edge, i.e., at a boundary between the aperture and the conducting surface, in this auxiliary problem by means of which one determines the current $\mathbf{J}$ on the surface $\mathcal{S}$ of the slotted cylinder due to the impressed current $\mathbf{J}^{\rm imp}$ $(=-\mathbf{J}^{\rm sc})$ in the aperture $\mathcal{A}$. We claim that $\mathbf{J}^{\rm imp}$ in $\mathcal{A}$ and $\mathbf{J}$ on $\mathcal{S}$ must together form a continuous function at the common edge. If these currents were not equal at the edge, a line charge would reside there in order to complete the electrical system, and this line charge would create an unbounded electric field, too singular to be physically acceptable. Thus, the impressed current in $\mathcal{A}$ must be equal to the induced current on $\mathcal{S}$ at the common aperture-conductor edge.

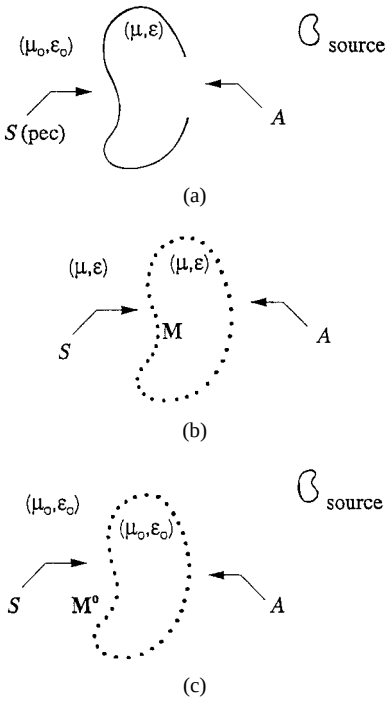

Fig. 4. Illustrations for the equivalent current method. (a) Original structure. (b) Interior equivalent model. (c) Exterior equivalent model.

The penetrated field is

$$\mathbf{E}^{\rm pen}(\boldsymbol{\rho}) = -\frac{\eta}{4k}\left[k^2\int_{C_S} J_l(\boldsymbol{\rho}')\hat{\mathbf{l}}' H_0^{(2)}(k|\boldsymbol{\rho}-\boldsymbol{\rho}'|)\,dl' + \nabla\int_{C_S}\frac{d}{dl'}J_l(\boldsymbol{\rho}')H_0^{(2)}(k|\boldsymbol{\rho}-\boldsymbol{\rho}'|)\,dl'\right] - \frac{\eta}{4k}\left[k^2\int_{C_A} J_l^{\rm imp}(\boldsymbol{\rho}')\hat{\mathbf{l}}' H_0^{(2)}(k|\boldsymbol{\rho}-\boldsymbol{\rho}'|)\,dl' + \nabla\int_{C_A}\frac{d}{dl'}J_l^{\rm imp}(\boldsymbol{\rho}')H_0^{(2)}(k|\boldsymbol{\rho}-\boldsymbol{\rho}'|)\,dl'\right] \tag{17}$$

where in (17) both J_l and $J_l^{\rm imp}$ are known currents. $J_l^{\rm imp}$ is known from the solution of (13) or (14) and J_l is known from the solution of (16).

C. Equivalent Current Method

In the equivalent current method, we propose an electromagnetic model valid in the interior region and another valid in the exterior and we utilize the equivalence principle to express field components valid for the interior and exterior regions. This method is based on satisfying the conditions that the tangential component of electric field be zero on the surfaces of the conducting body and that both the electric and magnetic fields be continuous through the aperture. Of course, the field components of the exterior model must satisfy the radiation condition.

The equivalent interior and exterior models are displayed in Fig. 4. In the *interior* equivalent model of Fig. 4(b), we place magnetic currents $\mathbf{M}$ in the region $\mathcal{A}$ *and* over the surface $\mathcal{S}$. The region outside $(\mathcal{S}+\mathcal{A})$ is then filled with material characterized by that of the interior region (μ,ε). For the

exterior equivalent model of Fig. 4(c), we place equivalent magnetic currents $\mathbf{M^o}$ over $\mathcal{A}$ *and* over $\mathcal{S}$ and the inside region is then filled with material characterized by that of the exterior region (μ_o, ε_o). Even though the slotted cylinder is a perfect electric conductor there are no electric currents involved in the formulation. The fields must satisfy

$$\mathcal{E}^{-}_{\tan}[\mathbf{M};\mathbf{r};\mathcal{S}^{-}+\mathcal{A}^{-}]=\mathbf{0}, \qquad \mathbf{r}\in\mathcal{S}^{-} \tag{18}$$

$$\mathcal{E}^{o^+}_{\tan}[\mathbf{M^o};\mathbf{r};\mathcal{S}^{+}+\mathcal{A}^{+}]+\mathbf{E}^{i}_{\tan}(\mathbf{r})=\mathbf{0}, \quad \mathbf{r}\in\mathcal{S}^{+} \tag{19}$$

$$\mathcal{E}^{-}_{\tan}[\mathbf{M};\mathbf{r};\mathcal{S}^{-}+\mathcal{A}^{-}]=\mathcal{E}^{o^+}_{\tan}[\mathbf{M^o};\mathbf{r};\mathcal{S}^{+}+\mathcal{A}^{+}]+\mathbf{E}^{i}_{\tan}(\mathbf{r}) \qquad \mathbf{r}\in\mathcal{A} \tag{20}$$

$$\mathcal{H}_{\tan}[\mathbf{M};\mathbf{r};\mathcal{S}+\mathcal{A}]=\mathcal{H}^{o}_{\tan}[\mathbf{M^o};\mathbf{r};\mathcal{S}+\mathcal{A}]+\mathbf{H}^{i}_{\tan}(\mathbf{r}) \qquad \mathbf{r}\in\mathcal{A} \tag{21}$$

where $\mathcal{E}[\mathbf{M};\mathbf{r};\Sigma]$ and $\mathcal{H}[\mathbf{M};\mathbf{r};\Sigma]$ can be expressed in terms of potentials as

$$\begin{aligned}\mathcal{E}[\mathbf{M};\mathbf{r};\Sigma]&=-\frac{1}{\varepsilon}\nabla\times\mathbf{F}(\mathbf{r})\\&=-\iint_{\Sigma}\mathbf{M}(\mathbf{r}')\times\nabla'_s G(\mathbf{r};\mathbf{r}')\,dS', \quad \mathbf{r}\neq\mathbf{r}'\end{aligned} \tag{22}$$

and

$$\mathcal{H}[\mathbf{M};\mathbf{r};\Sigma]=-j\omega\mathbf{F}(\mathbf{r})-\nabla\Psi(\mathbf{r}) \tag{23}$$

with

$$\begin{aligned}\mathbf{F}(\mathbf{r})&=\varepsilon\iint_{\Sigma}\mathbf{M}(\mathbf{r}')G(\mathbf{r};\mathbf{r}')\,dS'\\\Psi(\mathbf{r})&=\frac{j}{k\eta}\iint_{\Sigma}(\nabla'_s\cdot\mathbf{M}(\mathbf{r}'))G(\mathbf{r};\mathbf{r}')\,dS'\end{aligned} \tag{24}$$

in which $G(\mathbf{r};\mathbf{r}')$ is the free-space Green's function, $\eta=\sqrt{\mu/\varepsilon}$, and $k=\omega\sqrt{\mu\varepsilon}$. The "$o$" superscript simply indicates that a quantity so identified pertains to the exterior model, as opposed to the interior model. Expressions for $\mathcal{E}^{o}[\mathbf{M};\mathbf{r};\Sigma]$ and $\mathcal{H}^{o}[\mathbf{M};\mathbf{r};\Sigma]$ are similar to those in (22)–(24) but with μ, ε, k, and η replaced by μ_o, ε_o, k_o, and η_o, respectively. The minus (plus) superscripts in (18)–(20) indicate that the tangential electric field is evaluated in the limit as the field point $\mathbf{r}$ approaches the surface magnetic current from the interior (exterior) region of either model. Because it is not discontinuous at a surface magnetic current, such precaution is not needed in the case of a tangential component of magnetic field.

If we again consider the slotted cylinder shown in Fig. 2 excited by the same H-polarized incident plane wave, then the equivalent magnetic currents $\mathbf{M}$ and $\mathbf{M^o}$ are only in the z direction. Equations (18)–(21) for the slotted cylinder become

$$\begin{aligned}&\frac{1}{2\pi}M_z(\boldsymbol{\rho})-\frac{k}{4j}\int_{C_S+C_A}M_z(\boldsymbol{\rho}')\cos\theta H_1^{(2)}(k|\boldsymbol{\rho}-\boldsymbol{\rho}'|)\,dl'\\&\quad=0, \quad \boldsymbol{\rho}\in C_S\end{aligned} \tag{25}$$

$$\begin{aligned}&-\frac{1}{2\pi}M^o_z(\boldsymbol{\rho})-\frac{k_o}{4j}\int_{C_S+C_A}M^o_z(\boldsymbol{\rho}')\cos\theta H_1^{(2)}(k_o|\boldsymbol{\rho}-\boldsymbol{\rho}'|)\,dl'\\&\quad=-E^i_t(\boldsymbol{\rho}), \quad \boldsymbol{\rho}\in C_S\end{aligned} \tag{26}$$

$$\begin{aligned}&\frac{1}{2}M_z(\boldsymbol{\rho})-\frac{k}{4j}\int_{C_S+C_A}M_z(\boldsymbol{\rho}')\cos\theta H_1^{(2)}(k|\boldsymbol{\rho}-\boldsymbol{\rho}'|)\,dl'\\&\quad+\frac{1}{2\pi}M^o_z(\boldsymbol{\rho})+\frac{k_o}{4j}\int_{C_S+C_A}M^o_z(\boldsymbol{\rho}')\cos\theta\\&\quad\times H_1^{(2)}(k_o|\boldsymbol{\rho}-\boldsymbol{\rho}'|)\,dl'=E^i_t(\boldsymbol{\rho}), \quad \boldsymbol{\rho}\in C_A\end{aligned} \tag{27}$$

$$\begin{aligned}&-\frac{k}{4\eta}\int_{C_S+C_A}M_z(\boldsymbol{\rho}')H_0^{(2)}(k|\boldsymbol{\rho}-\boldsymbol{\rho}'|)\,dl'\\&\quad+\frac{k_o}{4\eta_o}\int_{C_S+C_A}M^o_z(\boldsymbol{\rho}')H_0^{(2)}(k_o|\boldsymbol{\rho}-\boldsymbol{\rho}'|)\,dl'\\&\quad=H^i_z(\boldsymbol{\rho}), \quad \boldsymbol{\rho}\in C_A.\end{aligned} \tag{28}$$

$\hat{\mathbf{n}}$ is the outward normal defined in Fig. 1 and $\cos\theta=\hat{\mathbf{u}}\cdot\hat{\mathbf{n}}$ with $\hat{\mathbf{u}}=(\boldsymbol{\rho}-\boldsymbol{\rho}')/|\boldsymbol{\rho}-\boldsymbol{\rho}'|$. For a surface with a discontinuous radius of curvature, the comment following (15) [18] should be observed. Note that (25)–(28) appear to be four equations in two unknowns, but this is not actually the case. One may view $\mathbf{M}$ and $\mathbf{M^o}$ over C_S as different from the same currents over C_A

$$\mathbf{M}=\begin{cases}\mathbf{M_s}, & \boldsymbol{\rho}\in C_S\\ \mathbf{M_a}, & \boldsymbol{\rho}\in C_A\end{cases} \tag{29}$$

and

$$\mathbf{M^o}=\begin{cases}\mathbf{M^o_s}, & \boldsymbol{\rho}\in C_S\\ \mathbf{M^o_a}, & \boldsymbol{\rho}\in C_A\end{cases}. \tag{30}$$

Once the interior and exterior equivalent currents have been determined, the correct interior and exterior fields can be calculated from the appropriate model. Referring to the interior model of Fig. 4(b), one can use the interior equivalent current found in (25)–(28) to solve for the correct interior field. Thus

$$\mathbf{E}^{\text{pen}}(\boldsymbol{\rho})=-\frac{k}{4j}\int_{C_S+C_A}M_z(\boldsymbol{\rho}')[\hat{\mathbf{z}}\times\hat{\mathbf{u}}]H_1^{(2)}(k|\boldsymbol{\rho}-\boldsymbol{\rho}'|)\,dl'. \tag{31}$$

where $\hat{\mathbf{u}}=(\boldsymbol{\rho}-\boldsymbol{\rho}')/|\boldsymbol{\rho}-\boldsymbol{\rho}'|$ is the direction of the vector from the source point $\boldsymbol{\rho}'$ on the cylinder to the observation point $\boldsymbol{\rho}$ in the interior of the cylinder.

III. Numerical Scheme

In this section, the integral equations are converted into matrix equations that can be solved on a computer. The first step in our moment-method solution [19] is to discretize the geometry and approximate the unknown current over the contour. The unknown current is expanded in a linear combination of basis functions and the resulting integral equations are then tested in order to obtain equations to solve for the unknown basis function coefficients.

A. Scatterer Method

We discretize the contour C_S into $(N+1)$ subdomains. The induced current on the surface is approximated by a linear combination of N piecewise linear functions with unknown current coefficients $\{J_n\}$. The piecewise linear basis functions (triangles) are ideal for accurately representing the unknown electric current induced on the cylinder for the TE case. They not only help to alleviate the difficulty of the derivative in the

equation, but they also lend themselves to the condition that the current goes to zero at the slot edges. In order to solve for the N unknown coefficients, the linear expansion functions are substituted into (5) and the equation is tested with a pulse function centered at $\boldsymbol{\rho}_m$. When the substitutions are made, the resulting equation can be written in matrix form as

$$[Z_{mn}][J_n] = [V_m] \tag{32}$$

in which $[J_n]$ is a column vector containing the unknown current coefficients and $[Z_{mn}]$ is a matrix whose elements are

$$\begin{aligned} Z_{mn} = -\frac{\eta}{4k}\Bigg\{ & \frac{k^2}{2}\Bigg[(\Delta_{m^-}\hat{\mathbf{l}}_{m^-} + \Delta_{m^+}\hat{\mathbf{l}}_{m^+}) \\ & \cdot \Bigg[\hat{\mathbf{l}}_{n^-}\int_{-\frac{1}{2}\Delta_{n^-}}^{0} H_0^{(2)}(k|\boldsymbol{\rho}_m - \boldsymbol{\rho}_n - l'\hat{\mathbf{l}}_{n^-}|)\,dl' \\ & + \hat{\mathbf{l}}_{n^+}\int_{0}^{\frac{1}{2}\Delta_{n^+}} H_0^{(2)}(k|\boldsymbol{\rho}_m - \boldsymbol{\rho}_n - l'\hat{\mathbf{l}}_{n^+}|)\,dl'\Bigg]\Bigg] \\ & + \frac{1}{\Delta_{n^-}}\int_{-\Delta_{n^-}}^{0}\big[H_0^{(2)}(k|\boldsymbol{\rho}_{m+\frac{1}{2}} - \boldsymbol{\rho}_n - l'\hat{\mathbf{l}}_{n^-}|) \\ & - H_0^{(2)}(k|\boldsymbol{\rho}_{m-\frac{1}{2}} - \boldsymbol{\rho}_n - l'\hat{\mathbf{l}}_{n^-}|)\big]\,dl' \\ & - \frac{1}{\Delta_{n^+}}\int_{0}^{\Delta_{n^+}}\big[H_0^{(2)}(k|\boldsymbol{\rho}_{m+\frac{1}{2}} - \boldsymbol{\rho}_n - l'\hat{\mathbf{l}}_{n^+}|) \\ & - H_0^{(2)}(k|\boldsymbol{\rho}_{m-\frac{1}{2}} - \boldsymbol{\rho}_n - l'\hat{\mathbf{l}}_{n^+}|)\big]\,dl'\Bigg\} \end{aligned} \tag{33}$$

where Δ_{p^-} is the length of the subsection extending from the $(p-1)$th subcontour endpoint to the pth subcontour endpoint, Δ_{p^+} is the length of the subsection extending from the pth subcontour endpoint to the $(p+1)$th subcontour endpoint, $\hat{\mathbf{l}}_{p^-}$ is the unit vector from the $(p-1)$th subcontour endpoint to the pth subcontour endpoint, and $\hat{\mathbf{l}}_{p^+}$ is the unit vector from the pth subcontour endpoint to the $(p+1)$th subcontour endpoint. The first two integrals of (33) result from approximations of the integral of the triangle basis functions by an equal-area unit-amplitude pulse function to facilitate integration, while the second pair reflects the piecewise constant derivative of the triangle basis function employed to represent the current J_l. $[V_m]$ is a column vector whose elements are values of the incident field tangential to the contour tested with the mth pulse function

$$\begin{aligned} V_m = -E_o^i\Bigg\{ & [-\cos\phi^i\hat{\mathbf{l}}_{m^-}\cdot\hat{\mathbf{y}} + \sin\phi^i\hat{\mathbf{l}}_{m^-}\cdot\hat{\mathbf{x}}]\frac{\Delta_{m^-}}{2} \\ & + [-\cos\phi^i\hat{\mathbf{l}}_{m^+}\cdot\hat{\mathbf{y}} + \sin\phi^i\hat{\mathbf{l}}_{m^+}\cdot\hat{\mathbf{x}}]\frac{\Delta_{m^-}}{2}\Bigg\} \\ & \times e^{jk(x_m\cos\phi^i + y_m\sin\phi^i)} \end{aligned} \tag{34}$$

where x_m and y_m are the Cartesian coordinates of $\boldsymbol{\rho}_m$.

The scattered field $\mathbf{E}^s$ can be computed by integrating over the induced current obtained from the integral equation solution

$$\begin{aligned} \mathbf{E}^s(\boldsymbol{\rho}) = -\frac{\eta}{4k}\Bigg[& k^2\int_{C_S} J_l(\boldsymbol{\rho}')\hat{\mathbf{l}}' H_0^{(2)}(k|\boldsymbol{\rho} - \boldsymbol{\rho}'|)\,dl' \\ & + \nabla\int_{C_S}\frac{d}{dl'}J_l(\boldsymbol{\rho}')H_0^{(2)}(k|\boldsymbol{\rho} - \boldsymbol{\rho}'|)\,dl'\Bigg]. \end{aligned} \tag{35}$$

The total field is computed as the sum of the scattered field above and the incident field

$$\mathbf{E}(\boldsymbol{\rho}) = \mathbf{E}^s(\boldsymbol{\rho}) + \mathbf{E}^i(\boldsymbol{\rho}) \tag{36}$$

where $\boldsymbol{\rho}$ is the field point. The gradient operator in (35) is replaced by its finite-difference approximation.

B. Short-Circuit Current Method

With a minor modification the numerical scheme used to implement the scatterer method can be employed in the short-circuit current method. One solves (13) or (14) using the method outlined above to determine the short-circuit current on the cylinder. The matrix equation can be written for this method as

$$\begin{bmatrix}[Z_{mn}^{aa}] & [Z_{mn}^{as}] \\ [Z_{mn}^{sa}] & [Z_{mn}^{ss}]\end{bmatrix}\begin{bmatrix}[J_n^a] \\ [J_n^s]\end{bmatrix} = \begin{bmatrix}[V_m^a] \\ [V_m^s]\end{bmatrix} \tag{37}$$

where $[J_n^a]$ and $[J_n^s]$ are the unknown current coefficients over the shorted aperture and conductor surfaces, respectively. The matrix elements $[Z_{mn}^{aa}]$, $[Z_{mn}^{as}]$, $[Z_{mn}^{sa}]$, and $[Z_{mn}^{ss}]$ represent the contributions from the shorted aperture to itself, the conductor to the shorted aperture, the shorted aperture to the conductor and the conductor to itself, respectively. $[V_m^a]$ and $[V_m^s]$ are the values of the tested incident electric field at $\boldsymbol{\rho}_m$ on the aperture and conductor surfaces, respectively.

Once the short-circuit current is available from the solution of (37), the equivalent E-field excitation $\mathbf{E}^{\text{imp}}$ is determined from

$$\begin{aligned} \mathbf{E}^{\text{imp}}(\boldsymbol{\rho}) = -\frac{\eta}{4k}\Bigg[& k^2\int_{C_A} J_l^{\text{imp}}(\boldsymbol{\rho}')\hat{\mathbf{l}}' H_0^{(2)}(k|\boldsymbol{\rho} - \boldsymbol{\rho}'|)\,dl' \\ & + \nabla\int_{C_A}\frac{d}{dl'}J_l^{\text{imp}}(\boldsymbol{\rho}')H_0^{(2)}(k|\boldsymbol{\rho} - \boldsymbol{\rho}'|)\,dl'\Bigg]. \end{aligned} \tag{38}$$

It is emphasized again that this impressed electric field is used to find the "*new*" impressed current on the cylinder. This is conveniently written in matrix form as

$$[Z_{mn}^{ss}][J_n] = -[Z_{mn}^{sa}][J_n^{\text{imp}}] \tag{39}$$

where $[J_n]$ is the unknown induced current, where $[J_n^{\text{imp}}]$ is the known impressed current equal and opposite to the aperture short-circuit current ($J^{\text{imp}} = -J^{\text{sc}}$) and where the right-hand side of (39) is the l component of equivalent E-field excitation. The penetrated field is simply the sum of the field due to the equivalent induced current on the conductor and that due to the impressed current in the aperture as indicated earlier in (17).

C. Equivalent Current Method

To solve (25)–(28), we discretize the contour C_S into N straight-line subsections ΔC_n that approximate the original contour and we approximate the equivalent magnetic current by a linear combination of N piecewise constant functions (pulses) with unknown current coefficients $\{M_n\}$. Substituting the current representation for the equivalent current into (25)–(28) and enforcing the new equations at match points $\boldsymbol{\rho}_m$ (collocation) located at the subcontour centers yield

$$\frac{M_m}{2} - \frac{k}{4j}\sum_{n=1}^{N^s+N^a} M_n\int_{\Delta C_n}\cos\theta_m H_1^{(2)}(k|\boldsymbol{\rho}_m - \boldsymbol{\rho}'|)\,dl' = 0, \qquad m = 1, 2, \cdots, N^s \tag{40}$$

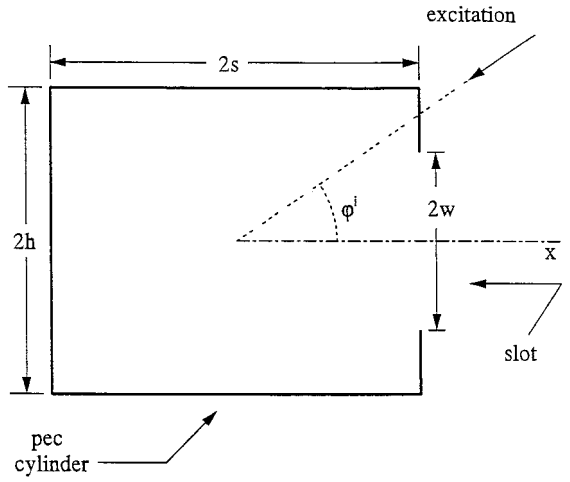

Fig. 5. Cross-sectional view of axially slotted rectangular conducting cylinder of side $2s$, height $2h$, and slot width $2w$ excited by plane wave.

$$\frac{M_m^o}{2}+\frac{k_o}{4j}\sum_{n=1}^{N^s+N^a} M_n^o\int_{\Delta C_n}\cos\theta_m H_1^{(2)}(k_o|\boldsymbol{\rho}_m-\boldsymbol{\rho}'|)\,dl' = E_l^i(\boldsymbol{\rho}_m),\quad m=1,2,\cdots,N^s \tag{41}$$

$$\frac{M_m}{2}-\frac{k}{4j}\sum_{n=1}^{N^s+N^a} M_n\int_{\Delta C_n}\cos\theta_m H_1^{(2)}(k|\boldsymbol{\rho}_m-\boldsymbol{\rho}'|)\,dl' + \frac{M_m^o}{2}+\frac{k_o}{4j}\sum_{n=1}^{N^s+N^a} M_n^o\int_{\Delta C_n}\cos\theta_m H_1^{(2)}(k_o|\boldsymbol{\rho}_m-\boldsymbol{\rho}'|)\,dl' = E_l^i(\boldsymbol{\rho}_m),\quad m=N^s+1,N^s+2,\cdots,N^s+N^a \tag{42}$$

$$-\frac{k}{4\eta}\sum_{n=1}^{N^a+N^s} M_n\int_{\Delta C_n} H_0^{(2)}(k|\boldsymbol{\rho}_m-\boldsymbol{\rho}'|)\,dl' + \frac{k_o}{4\eta_o}\sum_{n=1}^{N^a+N^s} M_n^o\int_{\Delta C_n} H_0^{(2)}(k_o|\boldsymbol{\rho}_m-\boldsymbol{\rho}'|)\,dl' = H_z^i(\boldsymbol{\rho}_m),\quad m=N^s+1,N^s+2,\cdots,N^s+N^a. \tag{43}$$

N^s is the number of unknowns over the conductor region and N^a is the number of current unknowns over the aperture region, while $\pm\frac{M_m}{2}$ represents the field contribution of the magnetic current M_m in the mth subsection to the tangential electric field in the same subdomain and $\cos\theta_m=\hat{\mathbf{u}}(\boldsymbol{\rho}_m)\cdot\hat{\mathbf{n}}(\boldsymbol{\rho}_m)$. The interior (penetrated) field is then determined from the interior equivalent currents as indicated earlier in (31).

IV. Results and Discussion

Computer codes have been developed for the scatterer method, equivalent current method, short-circuit current method, and combined-field short-circuit current method to determine currents from which the penetrated field can be calculated. To the extent possible, the currents determined from the codes were checked against known solutions or published data. The earliest published data concerning electric-field penetration into slotted conducting circular cylinders are due to Senior [4], [5]. Mautz and Harrington [13] determine the field amplitude $|E_\phi/\eta_o|$ at the center of a conducting circular cylinder as a function of ka for $\phi_o=5°$ and $\phi^i=0°$.

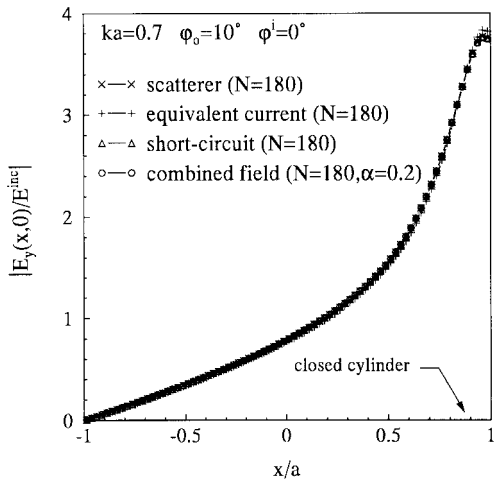

Fig. 6. Magnitude of y-directed (normalized) electric field on x axis of slotted circular cylinder excited by TE$_z$ plane wave [$ka=0.7$, $\phi_o=10°$, $\phi^i=0°$].

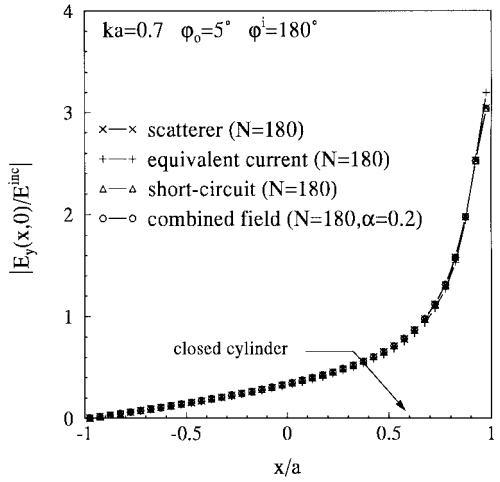

Fig. 7. Magnitude of y-directed (normalized) electric field on x axis of slotted circular cylinder excited by TE$_z$ plane wave [$ka=0.7$, $\phi_o=5°$, $\phi^i=180°$].

Fig. 10 of [13] is reproduced as accurately as possible for $\phi_o=5°$ and $ka\le 4.0$ in Fig. 10 of this work which is extended to include $4.0\le ka\le 6.0$.

To illustrate the methods of this paper and their relative accuracies, we select as a sample structure the axially slotted circular cylinder and axially slotted rectangular cylinder excited by TE (to cylinder and slot axes) incident plane waves. A cross-sectional view of the slotted circular conducting cylinder is found in Fig. 2 from which one observes that the cylinder radius is a, that the slot subtends an angle $2\phi_o$, and that an axially independent plane wave is incident at an angle ϕ^i measured with respect to the x axis. A cross-sectional view of the slotted rectangular conducting cylinder is depicted in Fig. 5. The cylinder length is $2s$, the cylinder height is $2h$, the slot width is $2w$, and an axially independent plane wave is incident at an angle ϕ^i measured with respect to the x axis.

Figs. 6 and 7 display the magnitude of the y-directed normalized electric field along the x axis of the slotted

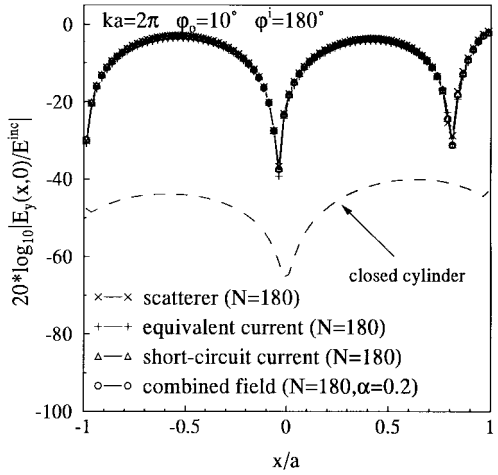

Fig. 8. Magnitude of y-directed (normalized) electric field on x axis of slotted circular cylinder excited by TE$_z$ plane wave [$ka = 2\pi$, $\phi_o = 10°$, $\phi^i = 180°$].

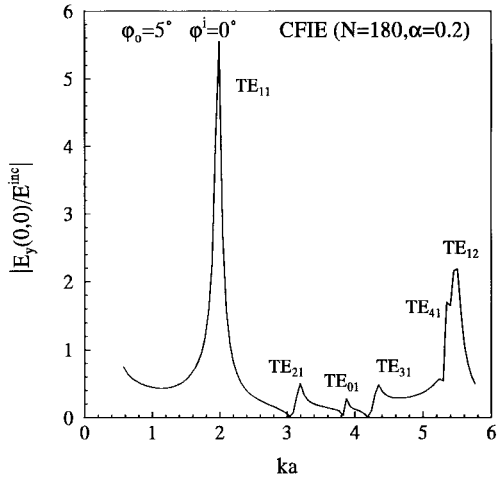

Fig. 10. Magnitude of y-directed (normalized) electric field at center of slotted circular cylinder excited by TE$_z$ plane wave for various ka[$\phi_o = 5°$, $\phi^i = 0°$].

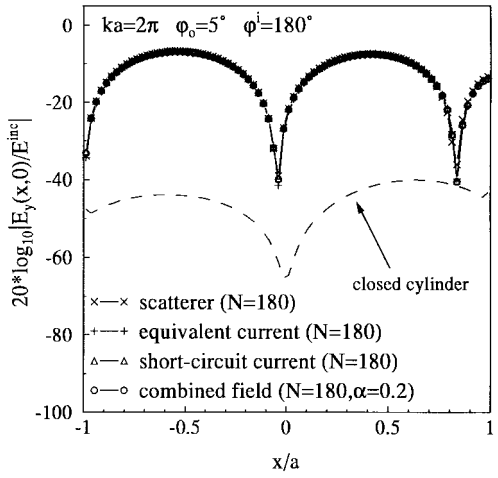

Fig. 9. Magnitude of y-directed (normalized) electric field on x axis of slotted circular cylinder excited by TE$_z$ plane wave [$ka = 2\pi$, $\phi_o = 5°$, $\phi^i = 180°$].

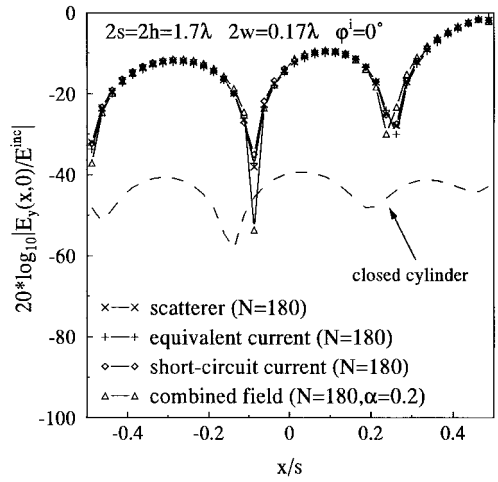

Fig. 11. Magnitude of y-directed (normalized) electric field on x axis of slotted square cylinder excited by TE$_z$ plane wave [$2s = 2h = 1.7\lambda$, $2w = 0.17\lambda$, $\phi^i = 0°$].

circular conducting cylinder of Fig. 2 excited by a plane wave for ($\phi_o = 10°, \phi^i = 0°$) and ($\phi_o = 5°, \phi^i = 180°$), respectively. The values of penetrated field calculated by means of the scatterer method, equivalent current method, short-circuit current method, and combined field short-circuit current method are nearly indistinguishable from one another. The y-directed normalized electric field along the x axis of a *closed* circular conducting cylinder ($ka = 0.7$), subject to a TE$_z$ incident plane wave ($\phi^i = 0°$), was determined from solutions of the EFIE in order to establish a reference value for the noise floor of the solution identified in figures as "closed cylinder." Of course, in all cases these values should be identically zero. Values of N in the figures indicate the number of unknowns employed to obtain a given solution and α is the value of the "combined-field solution parameter" of (8).

If the diameter of the circular cylinder is increased to $2a = 2\lambda$ ($ka = 2\pi$), the interior field distribution exhibits greater spatial variation than observed in the small cylinder cases. The log magnitude of the y-directed electric field along the x axis of a $ka = 2\pi$ slotted circular cylinder excited by a $\phi^i = 180°$ incident plane wave is presented in Figs. 8 and 9 for $\phi_o = 10°$ and $\phi_o = 5°$, respectively. When the slot angle is relatively large, good agreement is again obtained by all methods for the field penetration. Even if the slot angle is decreased to $\phi_o = 5°$, the agreement of the penetrated field determined by the three methods remains good.

When the field that penetrates through the slot is very small, comparable to the noise floor of the problem, the accuracy of the values given by the scatterer method very is poor. This error can be attributed to *subtractive cancellation*. Because the scattered electric field produced by the induced current on the cylinder and the incident electric field are almost of the same magnitude but opposite in sign, in order to yield a sum near zero, the sum of the two can be very inaccurate, leading to questionable results.

Fig. 10 shows the y-directed normalized electric field amplitude for various ka at the center of the circular cylinder

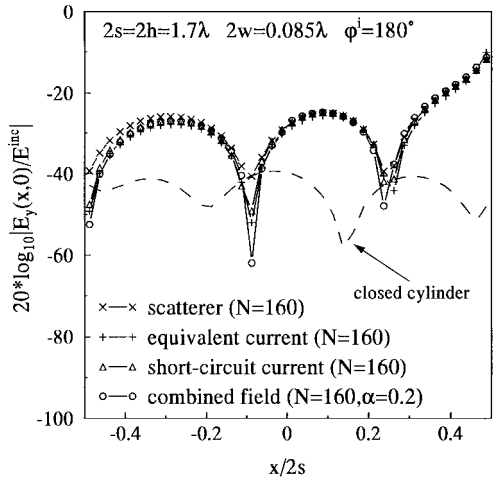

Fig. 12. Magnitude of y-directed (normalized) electric field on x axis of slotted square cylinder excited by TE_z plane wave [$2s = 2h = 1.7\lambda$, $2w = 0.085\lambda$, $\phi^i = 180°$].

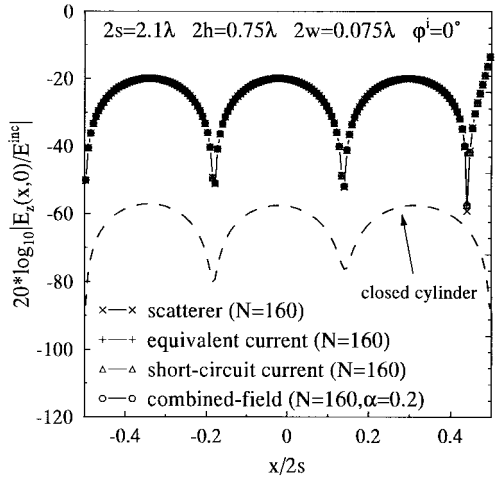

Fig. 13. Magnitude of y-directed (normalized) electric field on x axis of slotted rectangular cylinder excited by TE_z plane wave [$2s = 2.1\lambda$, $2h = 0.75\lambda$, $2w = 0.075\lambda$, $\phi^i = 0°$].

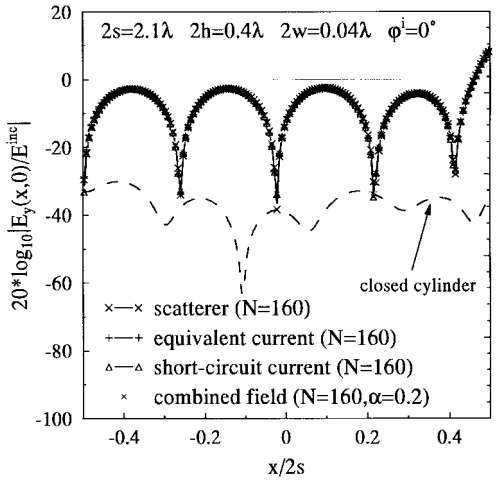

Fig. 14. Magnitude of y-directed (normalized) electric field on x axis of slotted rectangular cylinder excited by TE_z plane wave [$2s = 2.1\lambda$, $2h = 0.4\lambda$, $2w = 0.04\lambda$, $\phi^i = 0°$].

for $\phi_o = 5°$ and $\phi^i = 0°$. As can be clearly seen, specific near-modal solutions come to the fore as ka of the cylinder increases. The TE_{11} mode begins to dominate at $ka = 1.841$, the TE_{21} mode at $ka = 3.054$, the TE_{01} mode at $ka = 3.832$, the TE_{31} mode at $ka = 4.201$, the TE_{41} mode at $ka = 5.317$ and the TE_{12} mode at $ka = 5.331$.

The penetrated field along the x axis of a slotted square cylinder with $2s = 2h = 1.7\lambda$ and $2w = 0.17\lambda$ excited by a plane wave $(\phi^i = 0°)$ is presented in Fig. 11. The results from the different methods are found to be in good agreement. However, if the incident angle is changed to $\phi^i = 180°$ and the slot width is decreased to $2w = 0.085\lambda$, the field penetration determined by the scatterer method is less accurate (Fig. 12). The scatterer method fails because of the loss of accuracy in subtracting two nearly equal numbers.

In Fig. 13 is displayed the interior field distribution for a rectangular cylinder with $2s = 2.1\lambda$, $2h = 0.75\lambda$, $2w = 0.075\lambda$, and incident field angle $\phi^i = 0°$. Since this structure is effectively a shorted parallel-plate guide operating above cutoff for the TE_1 mode, standing wave patterns can exist and, indeed, are observed. In Fig. 14, the interior field distribution for a rectangular cylinder with $2s = 2.1\lambda$, $2h = 0.4\lambda$, $2w = 0.04\lambda$, and incident field angle $\phi^i = 0°$ is shown. Although this guide is below the TE cutoff, the TEM mode propagates in the guide and produces the standing wave patterns.

REFERENCES

[1] C. M. Butler, Y. Rahmat-Samii, and R. Mittra, "Electromagnetic penetration through apertures in conducting surfaces," *IEEE Trans. Antennas Propagat.*, vol. AP-26, pp. 82–93, Jan. 1978.

[2] J. J. Bowman, T. B. A. Senior, and P. L. E. Uslenghi, *Electromagnetic and Acoustic Scattering by Simple Shapes*. New York: Hemisphere, 1987, pp. 127–128.

[3] A. El-Hajj, K. Y. Kabalan, and R. F. Harrington, "Characteristic modes of a slot in a conducting cylinder and their use for penetration and scattering, TE case" *IEEE Trans. Antennas Propagat.*, vol. 40, pp. 156–161, Feb. 1992.

[4] T. B. A. Senior, "Field penetration into a cylindrical cavity," Univ. Michigan Radiation Lab., Ann Arbor, MI, Rep. 012643-2-T, Jan. 1975.

[5] ———, "Electromagnetic field penetration into a cylindrical cavity," *IEEE Trans. Electromagn. Compat.*, vol. 18, pp. 71–73, May 1976.

[6] H. K. Schuman and D. E. Warren, "Aperture coupling in bodies of revolution," *IEEE Trans. Antennas Propagat.*, vol. AP-26, pp. 778–783, Nov. 1978.

[7] S. A. Schelkunoff, "Kirchhoff's formula, its vector analogue and other field equivalence theorems," *Commun. Pure Appl. Math.*, vol. 4, pp. 43–59, June 1951.

[8] A. Taflove and K. Umashankar, "A hybrid moment method/finite-difference time-domain approach to electromagnetic coupling and aperture penetration into complex geometries," *IEEE Trans. Antennas Propagat.*, vol. AP-30, pp. 617–627, July 1982.

[9] J. A. Beren, "Diffraction of an H-polarized electromagnetic wave by a circular cylinder with an infinite axial slot," *IEEE Trans. Antennas Propagat.*, vol. AP-31, pp. 419–425, May 1983.

[10] W. A. Johnson and R. W. Ziolkowski, "The scattering of an H-polarized plane wave from an axially slotted infinite cylinder: A dual series approach," *Radio Sci.*, vol. 19, pp. 275–291, Jan./Feb. 1984.

[11] R. W. Ziolkowski, W. A. Johnson, and K. F. Casey, "Applications of Riemann-Hilbert problem techniques to electromagnetic coupling through apertures," *Radio Sci.*, vol. 19, pp. 1425–1431, Nov./Dec. 1984.

[12] R. W. Ziolkowski and J. B. Grant, "Scattering from cavity-backed apertures: The generalized dual series solution of the concentrically-loaded E-pol slit cylinder problem," *IEEE Trans. Antennas Propagat.*, vol. AP-35, pp. 504–528, May 1987.

[13] J. R. Mautz and R. F. Harrington, "Electromagnetic penetration into a conducting circular cylinder through a narrow slot, TE case," *J. Electromagn. Waves Applicat.*, vol. 3, no. 4, pp. 307–336, 1989.
[14] _____, "Electromagnetic penetration into a conducting circular cylinder through a narrow slot, TM case," *J. Electromagn. Waves Applicat.*, vol. 2, nos. 3/4, pp. 269–293, 1988.
[15] C. M. Butler, "Integral equation techniques for penetration through small apertures," in *Proc. Joint 3rd Int. Conf. Electromagn. Aerosp. Applicat. 7th Eur. Electromagn. Structures Conf.*, Torino, Italy, Sept. 1993, pp. 219–225.
[16] R. F. Harrington, *Time-Harmonic Electromagnetic Fields*. New York: McGraw-Hill, 1961.
[17] J. R. Mautz and R. F. Harrington, "H-field, E-field, and combined-field solutions for conducting bodies of revolution," *AEÜ*, vol. 32, pp. 157–164, 1978.
[18] N. Morita, N. Kumagai, and J. R. Mautz, *Integral Equation Methods in Electromagnetics*. Boston, MA: Artech House, 1990.
[19] R. F. Harrington, *Field Computation by Moment Methods*. Piscataway, NJ: IEEE Press, 1993.

John D. Shumpert (S'89) was born in Columbus, MS, on December 9, 1970. He received the B.S. and M.S. degrees in electrical engineering from Clemson University, Clemson, SC, in 1993 and 1995, respectively.

From 1993 to 1996, he was a National Science Foundation Graduate Fellow working on electromagnetic field penetration through small apertures in conducting surfaces and acoustic scattering from elastic cylinders. He is currently a Graduate Research Assistant in the Radiation Laboratory at the University of Michigan, Ann Arbor. His current research interests include frequency-selective surfaces, artificial dielectric structures for microwave and millimeter-wave applications, and photonic band-gap (PBG) materials.

Mr. Shumpert is a member of Phi Kappa Phi, Tau Beta Pi, Eta Kappa Nu, and Sigma Xi.

Chamlers M. Butler (S'55–M'63–SM'75–F'83), for a photograph and biography, see p. 1644 of the November 1997 issue of this TRANSACTIONS.